Am J Cancer Res 2023;13(4):1443-1456
www.ajcr.us /ISSN:2156-6976/ajcr0148557

Original Article

METTL3 regulates alternative splicing of cell cycle-related genes via crosstalk between mRNA m^{6}A modifications and splicing factors

Yeongjoo Kim[1,2*], Seungjae Shin[3*], Sunyoung Kwon[4,5*], Kisung Moon[4], Su-Vin Baek[6], Ahyoung Jo[6], Hyung-Sik Kim[6,7], Gue-Ho Hwang[8], Sangsu Bae[3,8], Yun Hak Kim[2,9], Sung-Yup Cho[3,8,10], Jung-Min Oh[6,7]

[1]Interdisplinary Program of Genomic Science, Pusan National University, Yangsan, Korea; [2]Department of Biomedical Informatics, School of Medicine, Pusan National University, Yangsan, Korea; [3]Department of Biomedical Sciences, Seoul National University College of Medicine, Seoul, Korea; [4]Department of Information Convergence Engineering, Pusan National University, Yangsan, Korea; [5]School of Biomedical Convergence Engineering, Pusan National University, Yangsan, Korea; [6]Department of Oral Biochemistry, Dental and Life Science Institute, School of Dentistry, Pusan National University, Yangsan, Korea; [7]Department of Life Science in Dentistry, School of Dentistry, Pusan National University, Yangsan, Korea; [8]Medical Research Center, Genomic Medicine Institute, Seoul National University College of Medicine, Seoul, Korea; [9]Department of Anatomy, School of Medicine, Pusan National University, Yangsan, Korea; [10]Cancer Research Institute, Seoul National University, Seoul, Korea. [*]Equal contributors and co-first authors.

Received December 16, 2022; Accepted March 9, 2023; Epub April 15, 2023; Published April 30, 2023

Abstract: N^6-methyladenosine (m^{6}A) modification in RNA affects various aspects of RNA metabolism and regulates gene expression. This modification is modulated by many regulatory proteins, such as m^{6}A methyltransferases (writers), m^{6}A demethylases (erasers), and m^{6}A-binding proteins (readers). Previous studies have suggested that alterations in m^{6}A regulatory proteins induce genome-wide alternative splicing in many cancer cells. However, the functional effects and molecular mechanisms of m^{6}A-mediated alternative splicing have not been fully elucidated. To understand the consequences of this modification on RNA splicing in cancer cells, we performed RNA sequencing and analyzed alternative splicing patterns in METTL3-knockdown osteosarcoma U2OS cells. We detected 1,803 alternatively spliced genes in METTL3-knockdown cells compared to the controls and found that cell cycle-related genes were enriched in differentially spliced genes. A comparison of the published MeRIP-seq data for METTL14 with our RNA sequencing data revealed that 70-87% of alternatively spliced genes had an m^{6}A peak near 1 kb of alternative splicing sites. Among the 19 RNA-binding proteins enriched in alternative splicing sites, as revealed by motif analysis, expression of SFPQ highly correlated with METTL3 expression in 12,839 TCGA pan-cancer patients. We also found that cell cycle-related genes were enriched in alternatively spliced genes of other cell lines with METTL3 knockdown. Taken together, we suggest that METTL3 regulates m^{6}A-dependent alternative splicing, especially in cell cycle-related genes, by regulating the functions of splicing factors such as SFPQ.

Keywords: Alternative splicing, cell cycle, m^{6}A modification, METTL3, splicing factor

Introduction

Epigenetic modifications, such as DNA methylation, RNA methylation, and histone modification, regulate gene expression patterns by controlling transcription or translation without causing any change in the DNA sequence. Among these modifications, N^6-methyladenosine (m^{6}A) is one of the most prevalent epigenetic modifications in eukaryotic RNA, which affects various aspects of RNA metabolism, such as RNA splicing, nuclear export, translation, and degradation [1]. Due to its widespread influence on RNA processing, m^{6}A modification needs to be finely controlled in cells, as abnormal m^{6}A modification is closely related to carcinogenesis [2]. The large number of proteins involved in m^{6}A modification are divided into three categories based on their function during the m^{6}A processing step: m^{6}A methyltransferases (writers), m^{6}A demethylases (erasers), and m^{6}A-binding proteins (readers) [3].

The first step of m^{6}A modification is performed by methyltransferase-like 3 (METTL3), METTL14, and Wilms Tumor 1 associated protein (WTAP) [4, 5]. The m^{6}A reader proteins, such as HNRNPA2B1, YTH N^6-methyladenosine RNA binding protein 1-3 (YTHDF1-3), YTH domain containing 1 (YTHDC1) and 2, and IGF2BP1-3, find m^{6}A-modified RNA and bind to it [6-9]. m^{6}A RNA modification is removed by m^{6}A eraser proteins, including fat mass and obesity-associated protein (FTO) and α-ketoglutarate-dependent dioxygenase alkB homolog 5 (ALKBH5) [10, 11].

RNA splicing is a pivotal step in eukaryotic RNA processing and is regulated by multiple factors, such as cis-acting elements and trans-acting factors. Alternative splicing is an essential mechanism for enhancing protein diversity within a limited genome. Finely controlled splicing is critical for gene regulation, and disruption of splicing by several stimuli or mutations can cause severe diseases [12-14].

In addition to direct mutations in DNA, m^{6}A modification of RNA also affects alternative splicing. Changes in m^{6}A controlling proteins, such as METTL3, FTO, YTHDC1, and ALKBH5, cause alternative splicing in the transcriptome [5, 10, 15, 16]. However, the functional consequences and molecular mechanism of m^{6}A-dependent alternative splicing are not fully understood. Therefore, we analyzed the global alternative splicing events in osteosarcoma U2OS cells with reduced METTL3 expression and investigated the m^{6}A peak locations and binding motifs of RNA-binding proteins (RBPs) near alternative splicing sites to determine the molecular mechanism and functional implication of the process.

Materials and methods

Cell culture and establishment of stable cell line

U2OS cells were purchased from the Korean Cell Line Bank. The cells were maintained in Dulbecco's modified Eagle's medium (Welgene, Korea) supplemented with 10% fetal bovine serum (Welgene, Korea), 1% penicillin, and streptomycin at 37°C and 5% CO_2. To generate METTL3-downregulated stable cell line, lenti-CRISPRv2 puro (Addgene #98290) containing a single guide RNA (sgNT: AAGATGAAAGGAAAGGCGTT, sgMETTL3: GAGCTTGGAATGGTCAGCAT), pCMV-VSVg (Addgene #8454), and psPAX2 (Addgene #12260) were co-transfected into the 293FT cell line using Lipofectamine 2000 (Thermo Fisher Scientific, MA, USA). The lentivirus-containing medium was collected at 48 h and 72 h and concentrated with a Lenti-X Concentrator (Takara, Japan) according to the manufacturer's protocol. U2OS cells were transduced with concentrated lentivirus along with polybrene and selected using puromycin for 3 days. After puromycin selection, single cells were seeded in 96-well culture plates. The knockdown efficiency of METTL3 was determined via western blotting. Cells were transfected with small interfering RNA targeting IGF2BP3 (IDT) using Lipofectamine 3000 Reagent (Thermo Fisher Scientific) according to the manufacturer's protocol.

Library construction and RNA sequencing

For RNA sequencing, total RNA was extracted using an RNeasy Plus Mini Kit (Qiagen). Libraries were constructed using TruSeq stranded mRNA (Illumina, CA, USA) and 1 μg of total RNA. The library was sequenced on the Illumina NovaSeq6000 platform with a 101 bp paired end model.

Western blot

Cells were lysed using RIPA buffer (Thermo Fisher Scientific) containing a protease inhibitor cocktail (Roche) and phosphatase inhibitor cocktail (Roche). The protein concentration was determined via the BCA assay (Thermo Fisher Scientific). Equal amounts of protein were loaded, separated via sodium dodecyl sulfate-polyacrylamide gel electrophoresis (SDS-PAGE), and transferred to nitrocellulose membranes. The membranes were blocked with 5% skim milk and incubated with anti-METTL3 (Cell Signaling Technology), anti-METTL14 (Cell Signaling Technology), and anti-β-actin (Sigma) antibodies at 4°C overnight. The membranes were probed with anti-rabbit IgG HRP-linked antibodies or anti-mouse IgG HRP-linked antibodies (Thermo Fisher Scientific). Protein bands were developed using the Scientific SuperSignal West Pico PLUS Chemiluminescent Substrate (Thermo Fisher Scientific). Western blot images were captured using Amersham Imager 680 (Cytiva).

RNA m^{6}A quantification

For quantification of RNA m^{6}A levels, total RNA was extracted using the RNeasy Plus Mini Kit (Qiagen) and estimated using the EpiQuik m^{6}A RNA Methylation Quantification Kit (Epigentek), according to the manufacturer's protocol.

Reverse transcription-polymerase chain reaction (RT-PCR)

Total RNA was extracted using TRIzol reagent (Thermo Fisher Scientific) according to the manufacturer's instructions. cDNA was synthesized from total isolated RNA using the SuperScript IV reverse transcriptase kit (Thermo Fisher Scientific), and RT-PCR was performed using Platinum PCR SuperMix High Fidelity (Thermo Fisher Scientific). The sequence of RT-PCR primers were MDM2 exon 1 Fwd: 5'-GGAGGGTAGACCTGTGGGCA-3', MDM2 exon 2 Rev: 5'-GGTCTCTTGTTCCGAAGCTG-3', LAMC3 exon 25 Fwd: 5'-CTCTTTCCTCCAGTGCCAAG-3', LAMC3 new exon 25 Fwd: 5'-TGCTGACTACTCCGCACTCA-3', LAMC3 exon 26 Rev: 5'-CTTCCTCCAGCTCCTGTCTG-3', CTNNB1 exon 15 Fwd: 5'-CACCCTGGTGCTGACTATCC-3', CTNNB1 exon 16 Rev: 5'-TCCCATAGGAAACTCAGCTTG-3', GTF3C1 exon 33 Fwd: 5'-AGCGCTCCAGGACTCAAAT-3', and GTF3C1 exon 34 Rev: 5'-CTGCCTGGGAGATGTTGG-3'. To estimate the mRNA expression, we performed real-time PCR using SYBR Green Master Mix (Bio-rad) and estimated mRNA level normalized by GAPDH used as internal control. The sequences of primers were as follows: IGF2BP3 Fwd: 5'-GAAGTTGAGCACTCGGTCCC-3', IGF2BP3 Rev: 5'-CAGTGTTCACTTGCTCACAGCT-3', SFPQ Fwd: 5'-GCCGAATGGGCTACATGGAT-3', SFPQ Rev: 5'-TCAGTACGCATGTCACTTCCC-3', GAPDH Fwd: 5'-ACCACAGTCCATGCCATCAC-3', and GAPDH Rev: 5'-TCCACCACCCTGTTGCTGTA-3'.

Analysis of alternative splicing events

Junction Usage Model (JUM) [17] is a computational software used for analyzing alternative pre-mRNA splicing patterns without annotations. For the execution of JUM (version 2.0.2), we aligned RNA-seq reads to the human (hg38) genome using the 2nd pass mapping method of STAR [18] to quantify splicing junctions accurately. Splicing junctions with at least five uniquely mapped reads in all replicates for each condition were filtered for alternative splicing analysis. Statistical cutoff with a *p*-value < 0.05 was considered to identify differential alternative splicing events between the tested conditions. Differential alternative splicing results were mapped to the known associated genes in the final process.

Preparation of m^{6}A peak and SFPQ dataset

The Gene Expression Omnibus (GEO) database was used to download GSE173519 and GSE113349. Adapter and quality trimming were performed with cutadapt (version 1.15) [19]. We removed reads with an error rate of over 0.2 and an adapter overlap of 1 after Illumina Small RNA 3' adapter trimming. Reads less than 12 bp were discarded. The reads that passed the above processes were aligned to the human genome version hg38 using bowtie2 (version 2.3.4.1) [20]. To investigate the general m^{6}A peak signature across samples, we combined the binding sites of m^{6}A writer complexes, such as METTL3, METTL14, and WTAP, and further analyses were performed.

Methylated RNA immunoprecipitation (MeRIP)-qPCR

MeRIP was performed using the published protocol with some modified [21]. Briefly, 10 μg of total RNA was fragmented with RNA fragmentation reagent (Thermo Fisher Scientific) at 94°C for 3 min and then 0.5 M EDTA was added immediately. Fragmented RNA was cleaned up with Oligo Clean & Concentration kit (Zymo research). After clean-up, 10% of fragmented RNA was collected as input. Remaining fragmented RNA was incubated with anti-m^{6}A (Synaptic System) or anti-mouse IgG (Santa Cruz biotechnology, Inc.) antibodies that were conjugated with protein A/G beads (Thermo Fisher Scientific) in MeRIP buffer (150 mM NaCl, 10 mM Tris-HCl (pH 7.5), 0.1% IGEPAL CA-630, and 40 U/μl RNasin® Ribonuclease Inhibitor (Promega)) at 4°C for 2 h. After immunoprecipitation, RNAs were washed 5 times with MeRIP buffer and eluted by competition with N^6-methyladenosine 5'-monophosphate (Santacruz biotechnology). Purified m^{6}A containing RNA was quantified by real-time PCR. SRAMP prediction model was used for prediction of m^{6}A site in SFPQ mature mRNA [22]. The sequence of MeRIP-qPCR primers were SFPQ Fwd: 5'-CGCCCTGTAATCCCAGCTACT-3', and SFPQ Rev: 5'-AGTCTCGCTCTGTTGTCCA-3'.

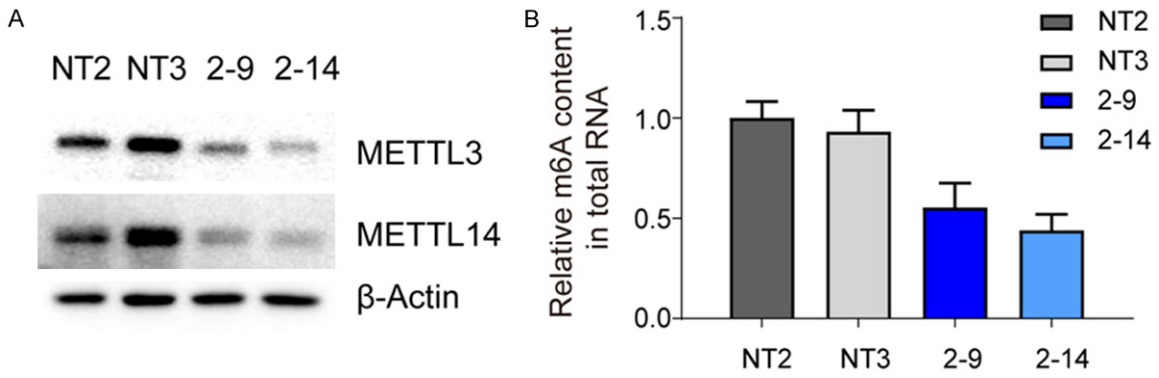

Figure 1. Establishment of stable METTL3-knockdown cell lines using osteosarcoma U2OS cells. A. Using the CRISPR-Cas9 system, METTL3-knockdown cells were established (2-9 and 2-14) along with control cells (NT2 and NT3). METTL3-knockdown efficiency was confirmed by the decreased METTL3 and METTL14 protein expression using western blot. B. Levels of m^{6}A in total RNA isolated from each stable cell line was measured via ELISA.

Ribonucleoprotein immunoprecipitation (RIP)-qPCR

RIP was performed using the published protocol with some modifications [23]. Cells were lysed with RIP lysis buffer (150 mM KCl, 10 mM Tris-HCl (pH 7.6), 2 mM EDTA, 0.5% NP-40, 0.5 mM DTT, 1:100 protease inhibitor cocktail, 400 U/ml RNase inhibitor). Lysate was incubated on ice and centrifuged at 13,200 rpm for 15 min to clear the lysate. 10% of lysate was collected as input. Remaining lysate was incubated anti-IGF2BP3 (Proteintech) or anti-rabbit IgG (cell Signaling Technology) antibodies that were conjugated with protein A/G beads (Thermo Fisher Scientific) in RIP lysis buffer at 4°C for overnight. After immunoprecipitation, RNAs were washed 5 times with washing buffer (200 mM NaCl, 50 mM Tris-HCl (pH 7.6), 2 mM EDTA, 0.05% NP-40, 0.5 mM DTT, 40 U/μl RNasin® Ribonuclease Inhibitor) and eluted by 150 μl elution buffer (10 μl 10% SDS, 10 μl Proteinase K, and 130 μl RIP lysis buffer) for 30 min at 55°C, and RNAs were purified using Trizol LS (Thermo Fisher Scientific). Purified RNA was quantified by real-time PCR for SFPQ mRNA used in MeRIP-qPCR.

Distance calculation between alternative splicing and m^{6}A writer complex/SFPQ binding site

The enriched signal peak of the aligned reads was identified using MACS2 (version 2.2.7.1) [24] with a minimal *q*-value of 0.05 and 0.01 for m^{6}A and SFPQ, respectively. Distances between peaks and their corresponding nearest alternative splicing events were calculated using closestBED, a component sub-package of Bedtools (version 2.26.0) [25].

Analysis of motif difference between gene groups

Alternative splicing events were uploaded to the rMAPS2 online tool [26], which can generate RNA maps of RBP binding sites. Acquired JUM output data were used to investigate the differences between alternatively spliced and non-alternatively spliced genes.

Gene ontology (GO) and KEGG pathway analysis

To determine the common molecular mechanism of alternatively spliced genes in METTL3-knockdown cells, we performed GO term and KEGG pathway analyses using DAVID functional annotation bioinformatics microarray analysis (http://david.ncifcrf.gov) [27, 28]. The top 10 enriched GO terms and KEGG pathways (p-value < 0.05) were identified.

Results

RNA-seq of METTL3-knockdown U2OS cell line

To understand the effect of m^{6}A RNA modification on mRNA splicing, we constructed a METTL3 stable knockdown osteosarcoma U2OS cell line using the CRISPR-Cas9 system. We confirmed decreased METTL3 protein expression in METTL3-knockdown stable cell lines 2-9 and 2-14 compared to the control cell lines NT2 and NT3 (**Figure 1A**). The expression of METTL14, the other component of the m^{6}A writer complex, was also decreased in cell lines 2-9 and 2-14 compared to the controls (**Figure 1A**). Furthermore, the level of total RNA m^{6}A methylation was also decreased in 2-9 and

2-14 cells compared with that in control cell lines (**Figure 1B**).

To investigate genome-wide alternative splicing changes in METTL3-knockdown cells, we performed RNA-seq with NT2, NT3, 2-9, and 2-14 cell lines. We obtained 79-89 million reads from sequencing, and ~80-90% reads were mapped to the human genome (UCSC, hg38). A total of 13,216 genes (FPKM > 1 in control samples) were included for further analysis. To ascertain the overall alternative splicing events in RNA-seq, we ran a junction usage model (JUM) [17]. Various alternative splicing events were discovered by JUM, including alternative 3' splice site (A3'SS), alternative 5' splice site (A5'SS), cassette exon, composite events, and intron retention (IR), and a total of 665-5519 splicing events were detected in each category (**Figure 2A**). As multiple alternative splicing events had occurred in one gene, the total number of genes with alternative splicing was 152-596 in each category (**Figure 2B**). A Venn diagram of the five alternative splicing categories at the gene level showed overlap between each splicing category (**Figure 2C**). This suggests that each gene has a dominant alternative splicing pattern and that the same type of alternative splicing event occurs several times in a particular gene. Next, we compared the upregulation or downregulation of the alternatively spliced genes in METTL3-knockdown cells to check for any correlation between splicing and gene expression changes. Results showed 521 and 897 upregulated and downregulated genes, respectively, in METTL3-knockdown cells compared to the control group (**Figure 2D**, fold change > 1.5, or < -1.5, $P < 0.05$). Among these genes, 57 upregulated (10.9%) and 70 downregulated genes (7.8%) had undergone alternative splicing events (**Figure 2D**), suggesting that some changes in gene expression could be influenced by alternative splicing modifications. To confirm the alternative splicing events detected via JUM analysis, we selected representative genes, and the alternative splicing patterns of these genes were validated via RT-PCR (**Figure 2E**).

GO terms and KEGG pathway analysis of alternatively spliced genes

To understand the biological function of genes with alternative splicing in METTL3-knockdown cells, we performed enriched GO terms and KEGG pathway analysis (**Figure 3**). The list of top 10 most enriched GO biological process (BP) showed that cell cycle-related functions, such as "cell division", "chromatin organization", "mitotic spindle organization", and "regulation of cell cycle", and some basic functions for gene expression, including "RNA splicing", "mRNA transport", "regulation of translation", and "proteasome-mediated ubiquitin-dependent protein catabolic process" were enriched in alternatively spliced genes (**Figure 3A**). The proteins encoded from these genes were localized in "cytosol", "nucleoplasm", "membrane", and "centrosome" (**Figure 3B**), and the enriched molecular function (MF) of these genes were "protein binding", "RNA binding", and "ATP-binding" functions (**Figure 3C**). Additionally, infection-related functions, such as *Escherichia* infection, *Salmonella* infection, and 'human T-cell leukemia virus 1 infection', were enriched based on the KEGG pathway analysis (**Figure 3D**). Since previous studies have demonstrated that decreased METTL3 inhibits the proliferation of osteosarcoma cells [29], we focused on "cell division" and "regulation of cell cycle" functions in our study. This suggests that changes in the alternative splicing of many cell cycle-related genes can affect the proliferation of osteosarcoma cells.

Comparison of m^{6}A peak and alternative splicing events

To determine whether the alternative splicing events observed in RNA-seq are related to METTL3 binding near alternative splicing sites, we compared our RNA-seq and MeRIP-seq data of the methyltransferase writer METTL14 (GSE173519) [30]. We first examined the presence of m^{6}A peaks from MeRIP-seq near 1 kb from alternative splicing sites found from our RNA-seq data (**Figure 4A**). We set up a 1 kb distance because the distance to which the U1 snRNP splicing factor can extend its influence in RNA is approximately 1 kb [31, 32]. Approximately 69.2-86.7% of alternatively spliced genes had an m^{6}A peak near 1 kb from alternative splicing sites in each category (q-value < 0.05; **Figure 4B**). The distance of the m^{6}A peak within 1 kb was further subdivided, showing that most of the m^{6}A peak (72.2-94.0%) was present within 200 bp of alternative splicing sites (**Figure 4C**). These data suggest that m^{6}A modification likely affects alternative splicing within very close distances.

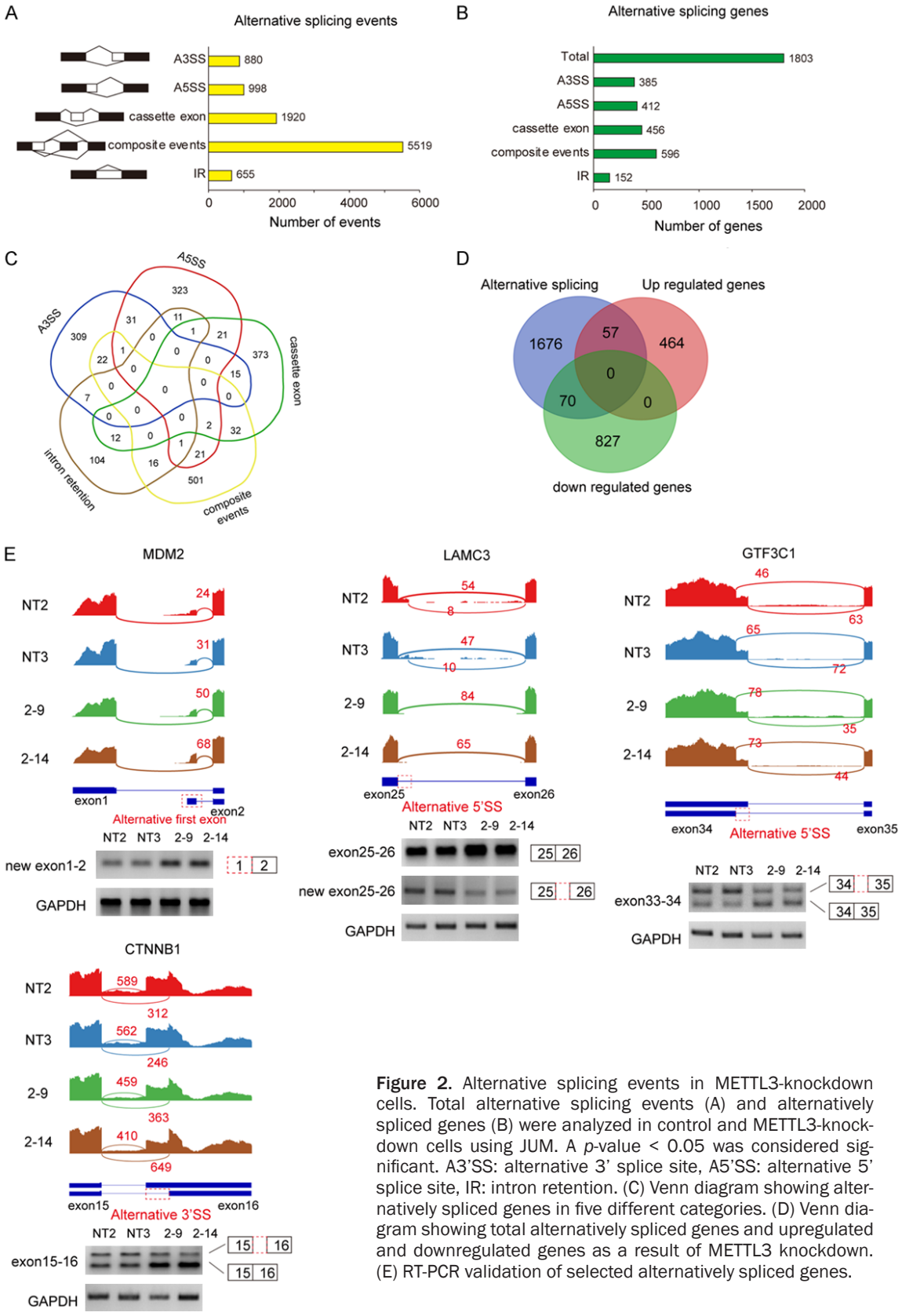

Figure 2. Alternative splicing events in METTL3-knockdown cells. Total alternative splicing events (A) and alternatively spliced genes (B) were analyzed in control and METTL3-knockdown cells using JUM. A *p*-value < 0.05 was considered significant. A3'SS: alternative 3' splice site, A5'SS: alternative 5' splice site, IR: intron retention. (C) Venn diagram showing alternatively spliced genes in five different categories. (D) Venn diagram showing total alternatively spliced genes and upregulated and downregulated genes as a result of METTL3 knockdown. (E) RT-PCR validation of selected alternatively spliced genes.

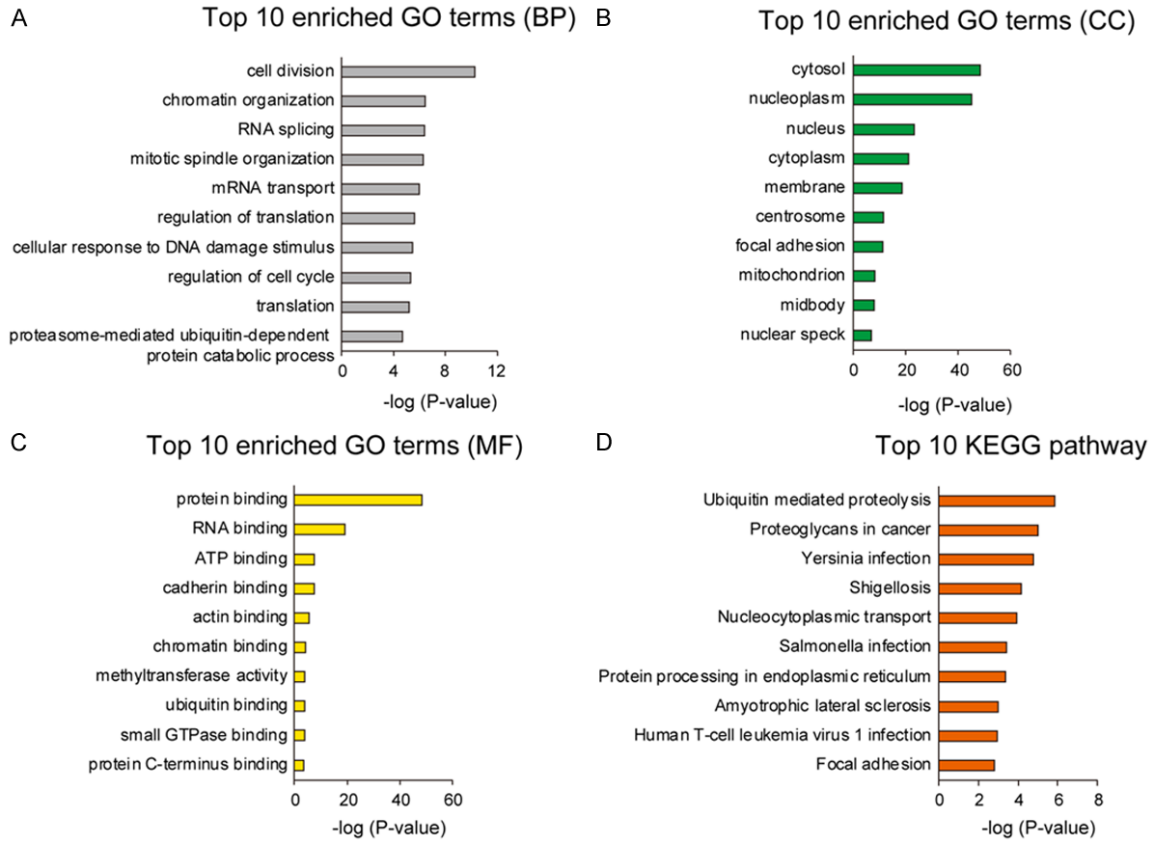

Figure 3. Gene Ontology (GO) term and KEGG pathway analyses of alternatively spliced genes. Top 10 enriched GO terms of alternatively spliced genes in biological process (A), cellular component (B), molecular function (C), and KEGG pathway (D). The bar graph represents the -log (*p*-value).

Analysis of RBP motif near alternative splicing sites

RBPs play an important role in regulating RNA splicing. To investigate the molecular mechanism underlying alternative splicing in METTL3-knockdown cells, we analyzed the effect of cis-acting elements and trans-acting factors on METTL3-related alternative splicing using RBP motif analysis. To search for enriched RBPs near alternative splicing sites in METTL3 knockdown cells, we performed RBP-binding motif analysis using rMAPS [33]. We discovered that the binding motifs of 19 RBPs were enriched near alternative splicing sites in METTL3 knockdown cells ($P < 0.05$; **Figure 5A**). To examine the relationship between the 19 RBPs and METTL3 expression in cancer, we analyzed the correlation between each RBP and METTL3 expression in 12,839 TCGA pan-cancer patients. Among the enriched 19 RBPs, seven showed considerable correlation with METTL3 expression (Pearson's correlation coefficient > 0.2) in cancer patients, with SFPQ showing the highest Pearson's correlation coefficient, 0.3368 (**Figure 5B**), thereby indicating that splicing factors, including SFPQ, affect alternative splicing in METTL3-knockdown cells. To investigate the m^{6}A-mediated regulation of SFPQ mRNA, we performed the methylated RNA immunoprecipitation (MeRIP)-qPCR for the predicted m^{6}A site in the 3'UTR of SFPQ mRNA and found that m^{6}As were significantly enriched in the 3'UTR of SFPQ mRNA (**Figure 5C**). As the mRNA levels of SFPQ were positively correlated with METTL3, an m^{6}A writer, we investigated the effect of IGF2BPs, which are involved in stabilizing m^{6}A-modified mRNAs [34] on the mRNA levels of SFPQ. Among the IGF2BPs, knockdown of IGF2BP3 significantly decreased the mRNA levels of SFPQ (**Figure 5D**) and IGF2BP3 was significantly enriched in the 3'UTR of SFPQ mRNAs in a ribonucleoprotein immunoprecipitation (RIP)-qPCR assay

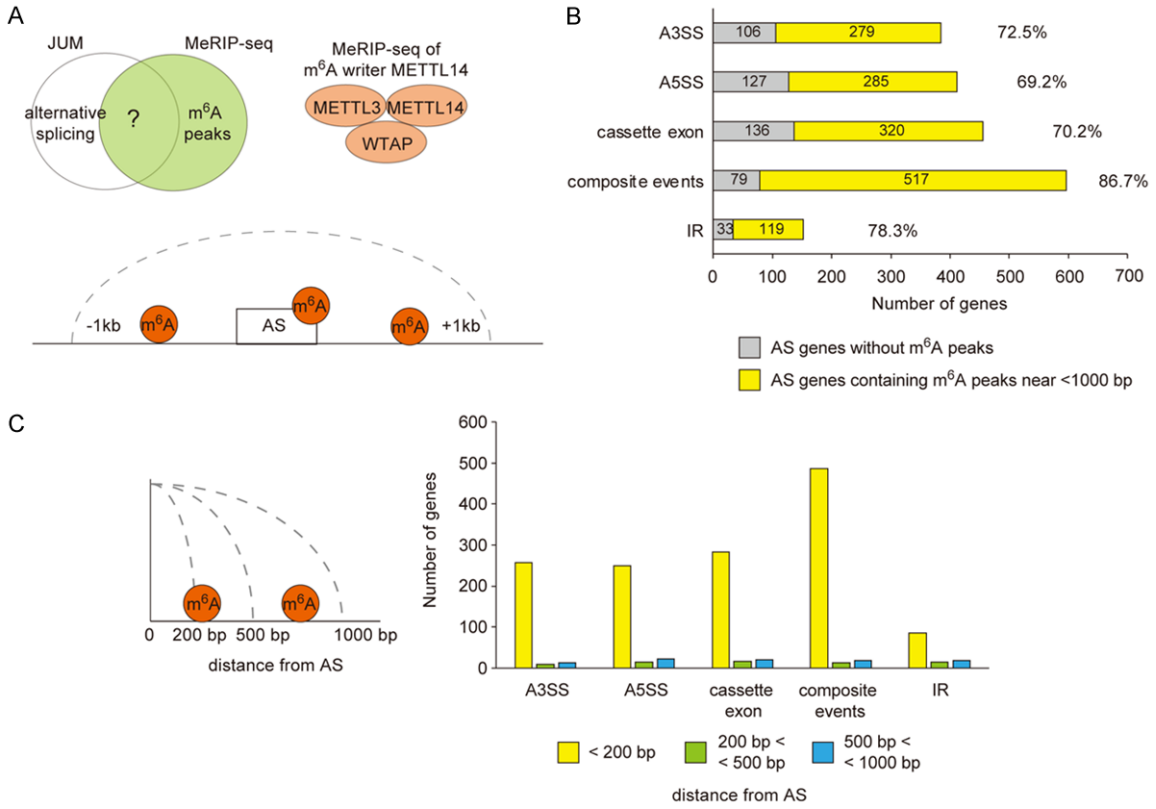

Figure 4. Analysis of m^{6}A peak location from MeRIP-seq data. A. Schematic diagram of the assay. To capture the m^{6}A peak near the alternatively spliced genes, we used MeRIP-seq data of the m^{6}A writer METTL14. B. The number of m^{6}A peaks located within a distance of 1 kb of alternatively spliced genes was counted. C. The m^{6}A peaks were further subdivided into categories based on the distance between the m^{6}A peak and alternatively spliced genes (< 200 bp, 200 bp-500 bp, and 500 bp-1 kb) and counted.

using an IGF2BP3 antibody (**Figure 5E**), suggesting that m^{6}A-modified SFPQ mRNAs are stabilized by the m^{6}A-binding protein IGF2BP3. To analyze the SFPQ binding near the alternative splicing site, we compared our RNA-seq and PAR-CLIP data of SFPQ (GSE113349) [35]. **Figure 5F** showed approximately 24.3-59.7% of alternatively spliced genes had a SFPQ binding peak near 1000 bp from the alternative splicing site in each category, suggesting that decent amount of alternative splicing was affected by SFPQ binding.

Comparison of alternatively spliced genes in different cell lines

To investigate whether there were any common alternatively spliced genes in METTL3-knockdown cells, we analyzed data from different cell lines in the GEO database (GSE183967 and GSE200649) [36]. Alternative splicing in HULEC-5a (endothelial cells; METTL3 was knocked down using shRNA) and A375 cells (melanoma cells; METTL3 was knocked down using shRNA) was analyzed using JUM with the same criteria as U2OS cells. The total number of alternatively spliced genes was 793 and 1072 in HULEC-5a and A375 cells, respectively (**Figure 6A**). We then compared the alternatively spliced genes in U2OS, HULEC-5a, and A375 cells (**Figure 6B**), where 39% (309/793) of alternatively spliced genes in HULEC-5a cells showed the same fate in U2OS or A375 cells. Furthermore, 33% (354/1072) of alternatively spliced genes in A375 cells and 24% (432/1803) in U2OS cells overlapped with those in the other cells (**Figure 6B**). To determine the enriched functions of alternatively spliced genes in HULEC-5a and A375 cells, we performed GO term analysis. Interestingly, similar to U2OS cells, “cell division” and “mitotic cell cycle” functions and “G2/M transition of the mitotic cell cycle” were enriched in HULEC-5a and A375 cells, respectively (**Figure 6C**).

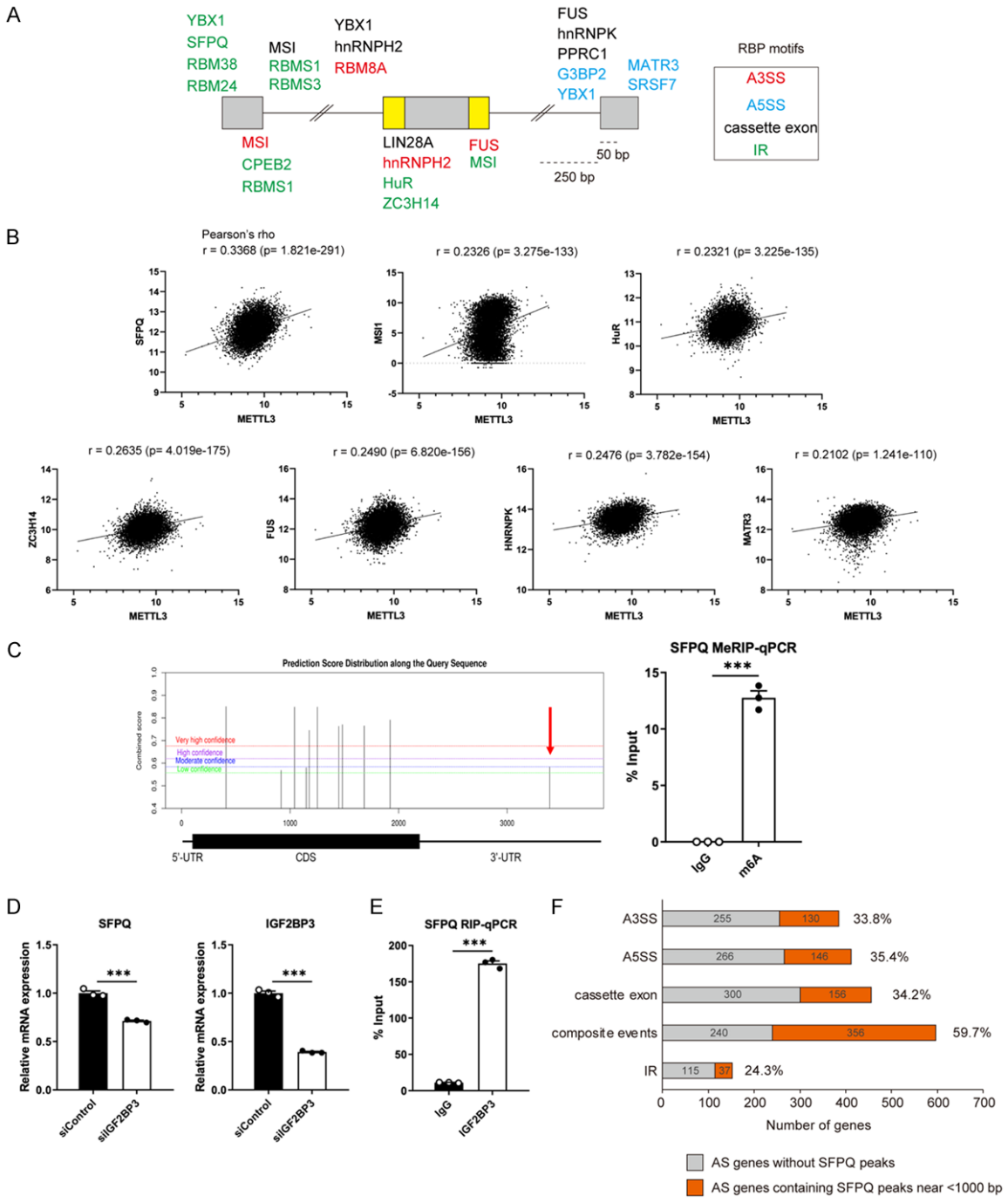

Figure 5. Enriched RBP motif in alternatively spliced genes. A. rMAPS captured a total of 19 RBPs that were enriched in alternatively spliced genes in METTL3-knockdown cells. Each RBP is represented with a different color based on the type of alternative splicing (alternative 3' splice site: red, alternative 5' splice site: blue, cassette exon: black, intron retention: green). B. The Pearson's correlation coefficients between each RBP and METTL3 expression were analyzed in 12,839 TCGA pan-cancer patients. C. The m^{6}A modification of the 3'UTR of SFPQ mRNA. The m^{6}A sites in SFPQ mRNA was analyzed using SRAMP (https://www.cuilab.cn/sramp; left panel) and a red arrow indicates the predicted m^{6}A site in the 3'UTR. MeRIP-qPCR analysis was performed to validate the predicted m^{6}A site in U2OS cells (right panel). D. The mRNA expression levels of SFPQ and IGF2BP3 after knockdown of IGF2BP3. The mRNA expression levels were estimated by real-time PCR after transfecting 25 nM of IGF2BP3 siRNA for 48 h. E. Enrichment of IGF2BP3 in the 3'UTR of SFPQ mRNA. RIP-qPCR analysis was performed to detect binding of IGF2BP3 to the 3'UTR of SFPQ mRNA. F. The number of SFPQ peaks located within a distance of 1000 bp of alternatively spliced genes was counted.

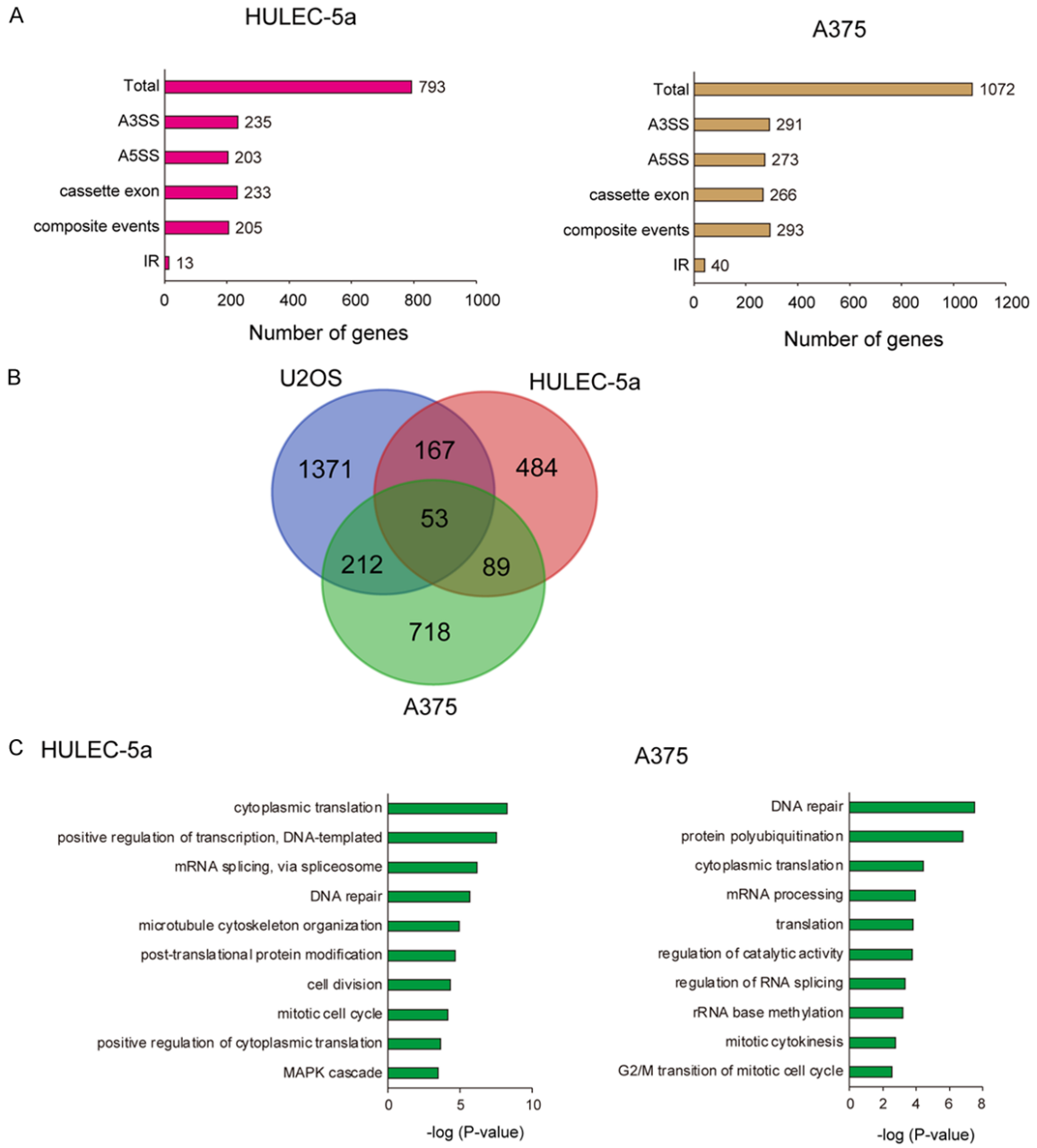

Figure 6. Alternatively spliced genes in METTL3-knockdown HULEC-5a and A375 cells. A. Alternative splicing was analyzed using JUM in METTL3-knockdown HULEC-5a and A375 cells using shRNA. The number of alternatively spliced genes is represented using a bar graph (p-value < 0.05 being significant). B. Venn diagram showing the number of common alternatively spliced genes between U2OS, HULEC-5a and A375 cells. C. Top 10 enriched GO terms of alternatively spliced genes in HULEC-5a and A375 cells.

Discussion

Splicing is regulated by multiple factors, with proper RNA splicing being an important factor in the regulation of gene expression in eukaryotes. Perturbed splicing in many genes due to defects in splicing factors has been reported in many cancers [12, 14, 37]. Therefore, understanding the mechanism underlying alternative splicing is important for cancer therapy. In addition to mutations in DNA and splicing factors, epigenetic modifications, such as m^6A, also affect alternative splicing. To understand the mechanism underlying alternative splicing by

m^{6}A modification, we used METTL3-knockdown U2OS cells and performed RNA-seq for analysis in this study. Our data showed that 1,803 genes demonstrated alternative splicing patterns in METTL3-knockdown cells compared to the control, with genes being enriched mostly in the "cell division" and "regulation of cell cycle" functions.

Many studies have reported reduced cell proliferation in osteosarcoma and other cancer cells with METTL3 knockdown [29, 38, 39] which can be explained by the enrichment of cell cycle-related function in alternatively spliced genes (**Figure 3A**). The enrichment of cell cycle-related functions in alternatively spliced genes was not only observed in U2OS cells with METTL3 knockdown but also in HULEC-5a and A375 cells (**Figure 6C**). It is well known that m^{6}A is involved in stem cell development and cell cycle regulation [40, 41]. Additionally, a recent study with dental pulp stem cells also showed that decreased METTL3 expression was associated with cell cycle and mitosis using m^{6}A RIP-seq and RNA-seq [42]. In the case of CCNB1, which is alternatively spliced in both U2OS and A375 cells, this modification has been reported to cause G2 and M phage lengthening in zebrafish [43]. MDM2 captured in both U2OS and A375 cells has been reported as an alternative and aberrant splicing in human cancer [44]. These data suggest that alternative splicing of cell cycle-related genes in METTL3-knockdown cells is not a cell type-specific phenomenon and, therefore, plays a significant role in cancer development.

The total decrease in m^{6}A modifications in RNA can affect alternative splicing in METTL3 knockdown. Many alternatively spliced genes, which varied 69.2-86.7% depending on the type of alternative splicing, have an m^{6}A peak near the splicing site (**Figure 4**). This suggests that, although not all alternatively spliced genes have m^{6}A peaks, alternative splicing of a considerable number of genes is regulated by an m^{6}A-dependent mechanism.

Although RNA m^{6}A modification has been suggested to be associated with the alternative splicing of mRNA, the detailed molecular mechanisms have not been fully elucidated. One of the main players in m^{6}A-dependent mRNA splicing is the m^{6}A reader protein, YTHDC1. This was reported to be localized in the nucleus and participate in the exon inclusion of targeted mRNAs in an m^{6}A-dependent manner by recruiting the splicing factor SRSF3 and inhibiting the splicing factor SRSF10 from binding to the mRNA [45]. In mouse oocytes, YTHDC1 deficiency resulted in extensive alternative splicing defects in association with splicing factors such as CPSF6, SRSF3, and SRSF7, and only in wild-type mice, but not m^{6}A-binding-deficient mice, YTHDC1 rescued this phenomenon [46]. Therefore, the m^{6}A reader YTHDC1-dependent recruitment of splicing factors is one of the possible mechanisms underlying m^{6}A-dependent alternative splicing.

When we analyzed the effect of cis-acting elements and trans-acting factors using enriched RBP motif analysis, 19 RBP motifs were found to be enriched near the alternative splicing site in METTL3-knockdown cells (**Figure 5A**). Among them, the expression of the splicing factor SFPQ showed the maximum correlation with METTL3 expression in 12,839 TCGA pan-cancer patients. SFPQ, an essential splicing factor, is involved in early spliceosome formation and alternative splicing [47]. It also participates in exon inclusion in association with the splicing factor heterogeneous nuclear ribonucleoprotein (hnRNP) M and NeuN [48, 49] but promotes exon skipping of the CD45 gene in association with the exonic splicing silencer 1 (ESS1)-bound hnRNP L complex [50]. Additionally, SFPQ is known as a direct binding partner of the FTO m^{6}A eraser protein, and the interaction between these two proteins enhances the demethylation of m^{6}A modification [51]. The enriched SFPQ motif near the alternative splicing site in METTL3-knockdown cells suggests that SFPQ might have a different function from the previously known demethylation function of FTO binding. Previous mass spectrometry data demonstrated that SFPQ acts as a binding partner of METTL3 based on immunoprecipitation analysis [52], thereby suggesting that the function of SFPQ is regulated by METTL3. In addition, METTL3 binds to SFPQ mRNA as per RIP-seq data [52], and the expression of SFPQ can be regulated by the binding of the m^{6}A reader proteins IGF2BP1/2/3 and YTHDF1/2 [6, 53]. We verified that the 3'UTR of SFPQ mRNAs was modified by m^{6}A, which was subsequently recognized by IGF2BP3, leading to the stabilization of SFPQ mRNA (**Figure 5C-E**). These data suggest that METTL3 regulates alternative splicing

by altering the function and expression of the splicing factor SFPQ via direct binding to the SFPQ protein or m^6A modification of SFPQ mRNA.

In summary, we observed genome-wide alternative splicing changes in METTL3-knockdown cells, and interestingly, cell cycle-related genes found to be enriched in METTL3-knockdown U2OS cells showed similar data in several different cell types. Our analysis suggests that a decent number of alternative splicing events can be regulated by direct m^6A modification by METTL3; however, m^6A peak-independent alternative splicing also occurs. Furthermore, the splicing factor SFPQ regulates alternative splicing in a METTL3-dependent manner.

Acknowledgements

This work was supported by a National Research Foundation of Korea (NRF) grant funded by the Korean government (MSIT) (No. NRF-2021R1C1C1005358, NRF-2021R1A2C3008021, and NRF-2018R1A5A2023879), and the Creative-Pioneering Researchers Program through Seoul National University (No. 800-20200510). S. Shin received a scholarship from BK21 FOUR Education Program.

Disclosure of conflict of interest

The authors declare that the research was conducted in the absence of any commercial or financial relationships that could be construed as a potential conflict of interest.

Address correspondence to: Yun Hak Kim, Department of Biomedical Informatics, School of Medicine, Pusan National University, Yangsan, Korea. Tel: +82-51-510-8091; E-mail: yunhak10510@pusan.ac.kr; Sung-Yup Cho, Department of Biomedical Sciences, Seoul National University College of Medicine, Seoul, Korea. Tel: +82-2-740-8241; E-mail: csybio@snu.ac.kr; Jung-Min Oh, Department of Oral Biochemistry, Dental and Life Science Institute, School of Dentistry, Pusan National University, Yangsan, Korea. Tel: +82-51-510-8226; E-mail: jminoh@pusan.ac.kr

References

[1] Jiang X, Liu B, Nie Z, Duan L, Xiong Q, Jin Z, Yang C and Chen Y. The role of m6A modification in the biological functions and diseases. Signal Transduct Target Ther 2021; 6: 74.

[2] Jones PA, Issa JP and Baylin S. Targeting the cancer epigenome for therapy. Nat Rev Genet 2016; 17: 630-641.

[3] Zaccara S, Ries RJ and Jaffrey SR. Reading, writing and erasing mRNA methylation. Nat Rev Mol Cell Biol 2019; 20: 608-624.

[4] Liu J, Yue Y, Han D, Wang X, Fu Y, Zhang L, Jia G, Yu M, Lu Z, Deng X, Dai Q, Chen W and He C. A METTL3-METTL14 complex mediates mammalian nuclear RNA N6-adenosine methylation. Nat Chem Biol 2014; 10: 93-95.

[5] Ping XL, Sun BF, Wang L, Xiao W, Yang X, Wang WJ, Adhikari S, Shi Y, Lv Y, Chen YS, Zhao X, Li A, Yang Y, Dahal U, Lou XM, Liu X, Huang J, Yuan WP, Zhu XF, Cheng T, Zhao YL, Wang X, Rendtlew Danielsen JM, Liu F and Yang YG. Mammalian WTAP is a regulatory subunit of the RNA N6-methyladenosine methyltransferase. Cell Res 2014; 24: 177-189.

[6] Wang X, Zhao BS, Roundtree IA, Lu Z, Han D, Ma H, Weng X, Chen K, Shi H and He C. N(6)-methyladenosine modulates messenger RNA translation efficiency. Cell 2015; 161: 1388-1399.

[7] Zhang Z, Theler D, Kaminska KH, Hiller M, de la Grange P, Pudimat R, Rafalska I, Heinrich B, Bujnicki JM, Allain FH and Stamm S. The YTH domain is a novel RNA binding domain. J Biol Chem 2010; 285: 14701-14710.

[8] Shi H, Wang X, Lu Z, Zhao BS, Ma H, Hsu PJ, Liu C and He C. YTHDF3 facilitates translation and decay of N(6)-methyladenosine-modified RNA. Cell Res 2017; 27: 315-328.

[9] Du H, Zhao Y, He J, Zhang Y, Xi H, Liu M, Ma J and Wu L. YTHDF2 destabilizes m(6)A-containing RNA through direct recruitment of the CCR4-NOT deadenylase complex. Nat Commun 2016; 7: 12626.

[10] Zheng G, Dahl JA, Niu Y, Fedorcsak P, Huang CM, Li CJ, Vagbo CB, Shi Y, Wang WL, Song SH, Lu Z, Bosmans RP, Dai Q, Hao YJ, Yang X, Zhao WM, Tong WM, Wang XJ, Bogdan F, Furu K, Fu Y, Jia G, Zhao X, Liu J, Krokan HE, Klungland A, Yang YG and He C. ALKBH5 is a mammalian RNA demethylase that impacts RNA metabolism and mouse fertility. Mol Cell 2013; 49: 18-29.

[11] Jia G, Fu Y, Zhao X, Dai Q, Zheng G, Yang Y, Yi C, Lindahl T, Pan T, Yang YG and He C. N6-methyladenosine in nuclear RNA is a major substrate of the obesity-associated FTO. Nat Chem Biol 2011; 7: 885-887.

[12] Oh JM, Venters CC, Di C, Pinto AM, Wan L, Younis I, Cai Z, Arai C, So BR, Duan J and Dreyfuss G. U1 snRNP regulates cancer cell migration and invasion in vitro. Nat Commun 2020; 11: 1.

[13] Ilagan JO, Ramakrishnan A, Hayes B, Murphy ME, Zebari AS, Bradley P and Bradley RK.

U2AF1 mutations alter splice site recognition in hematological malignancies. Genome Res 2015; 25: 14-26.
[14] Yoshida K, Sanada M, Shiraishi Y, Nowak D, Nagata Y, Yamamoto R, Sato Y, Sato-Otsubo A, Kon A, Nagasaki M, Chalkidis G, Suzuki Y, Shiosaka M, Kawahata R, Yamaguchi T, Otsu M, Obara N, Sakata-Yanagimoto M, Ishiyama K, Mori H, Nolte F, Hofmann WK, Miyawaki S, Sugano S, Haferlach C, Koeffler HP, Shih LY, Haferlach T, Chiba S, Nakauchi H, Miyano S and Ogawa S. Frequent pathway mutations of splicing machinery in myelodysplasia. Nature 2011; 478: 64-69.
[15] Zhao X, Yang Y, Sun BF, Shi Y, Yang X, Xiao W, Hao YJ, Ping XL, Chen YS, Wang WJ, Jin KX, Wang X, Huang CM, Fu Y, Ge XM, Song SH, Jeong HS, Yanagisawa H, Niu Y, Jia GF, Wu W, Tong WM, Okamoto A, He C, Rendtlew Danielsen JM, Wang XJ and Yang YG. FTO-dependent demethylation of N6-methyladenosine regulates mRNA splicing and is required for adipogenesis. Cell Res 2014; 24: 1403-1419.
[16] Dominissini D, Moshitch-Moshkovitz S, Schwartz S, Salmon-Divon M, Ungar L, Osenberg S, Cesarkas K, Jacob-Hirsch J, Amariglio N, Kupiec M, Sorek R and Rechavi G. Topology of the human and mouse m6A RNA methylomes revealed by m6A-seq. Nature 2012; 485: 201-206.
[17] Wang Q and Rio DC. JUM is a computational method for comprehensive annotation-free analysis of alternative pre-mRNA splicing patterns. Proc Natl Acad Sci U S A 2018; 115: E8181-E8190.
[18] Dobin A, Davis CA, Schlesinger F, Drenkow J, Zaleski C, Jha S, Batut P, Chaisson M and Gingeras TR. STAR: ultrafast universal RNA-seq aligner. Bioinformatics 2013; 29: 15-21.
[19] Martin M. Cutadapt removes adapter sequences from high-throughput sequencing reads. EMBnet Journal 2011; 17: 10-12.
[20] Langmead B and Salzberg SL. Fast gapped-read alignment with Bowtie 2. Nat Methods 2012; 9: 357-359.
[21] Dominissini D, Moshitch-Moshkovitz S, Salmon-Divon M, Amariglio N and Rechavi G. Transcriptome-wide mapping of N(6)-methyladenosine by m(6)A-seq based on immunocapturing and massively parallel sequencing. Nat Protoc 2013; 8: 176-189.
[22] Zhou Y, Zeng P, Li YH, Zhang Z and Cui Q. SRAMP: prediction of mammalian N6-methyladenosine (m6A) sites based on sequence-derived features. Nucleic Acids Res 2016; 44: e91.
[23] Peritz T, Zeng F, Kannanayakal TJ, Kilk K, Eiriksdottir E, Langel U and Eberwine J. Immunoprecipitation of mRNA-protein complexes. Nat Protoc 2006; 1: 577-580.
[24] Gaspar JM. Improved peak-calling with MACS2. BioRxiv 2018; 496521.
[25] Quinlan AR and Hall IM. BEDTools: a flexible suite of utilities for comparing genomic features. Bioinformatics 2010; 26: 841-842.
[26] Hwang JY, Jung S, Kook TL, Rouchka EC, Bok J and Park JW. rMAPS2: an update of the RNA map analysis and plotting server for alternative splicing regulation. Nucleic Acids Res 2020; 48: W300-W306.
[27] Huang da W, Sherman BT and Lempicki RA. Systematic and integrative analysis of large gene lists using DAVID bioinformatics resources. Nat Protoc 2009; 4: 44-57.
[28] Sherman BT, Hao M, Qiu J, Jiao X, Baseler MW, Lane HC, Imamichi T and Chang W. DAVID: a web server for functional enrichment analysis and functional annotation of gene lists (2021 update). Nucleic Acids Res 2022; 50: W216-W221.
[29] Zhou L, Yang C, Zhang N, Zhang X, Zhao T and Yu J. Silencing METTL3 inhibits the proliferation and invasion of osteosarcoma by regulating ATAD2. Biomed Pharmacother 2020; 125: 109964.
[30] Li HB, Huang G, Tu J, Lv DM, Jin QL, Chen JK, Zou YT, Lee DF, Shen JN and Xie XB. METTL14-mediated epitranscriptome modification of MN1 mRNA promote tumorigenicity and all-trans-retinoic acid resistance in osteosarcoma. EBioMedicine 2022; 82: 104142.
[31] Kaida D, Berg MG, Younis I, Kasim M, Singh LN, Wan L and Dreyfuss G. U1 snRNP protects pre-mRNAs from premature cleavage and polyadenylation. Nature 2010; 468: 664-668.
[32] Oh JM, Di C, Venters CC, Guo J, Arai C, So BR, Pinto AM, Zhang Z, Wan L, Younis I and Dreyfuss G. U1 snRNP telescripting regulates a size-function-stratified human genome. Nat Struct Mol Biol 2017; 24: 993-999.
[33] Park JW, Jung S, Rouchka EC, Tseng YT and Xing Y. rMAPS: RNA map analysis and plotting server for alternative exon regulation. Nucleic Acids Res 2016; 44: W333-338.
[34] Huang H, Weng H, Sun W, Qin X, Shi H, Wu H, Zhao BS, Mesquita A, Liu C, Yuan CL, Hu YC, Huttelmaier S, Skibbe JR, Su R, Deng X, Dong L, Sun M, Li C, Nachtergaele S, Wang Y, Hu C, Ferchen K, Greis KD, Jiang X, Wei M, Qu L, Guan JL, He C, Yang J and Chen J. Recognition of RNA N(6)-methyladenosine by IGF2BP proteins enhances mRNA stability and translation. Nat Cell Biol 2018; 20: 285-295.
[35] Yamazaki T, Souquere S, Chujo T, Kobelke S, Chong YS, Fox AH, Bond CS, Nakagawa S, Pierron G and Hirose T. Functional domains of NEAT1 architectural lncRNA induce paraspeckle assembly through phase separation. Mol Cell 2018; 70: 1038-1053, e7.

[36] Yue Z, Cao M, Hong A, Zhang Q, Zhang G, Jin Z, Zhao L, Wang Q, Fang F, Wang Y and Sun J. m(6)A methyltransferase METTL3 promotes the progression of primary acral melanoma via mediating TXNDC5 methylation. Front Oncol 2022; 11: 770325.
[37] Oltean S and Bates DO. Hallmarks of alternative splicing in cancer. Oncogene 2014; 33: 5311-5318.
[38] Hou H, Zhao H, Yu X, Cong P, Zhou Y, Jiang Y and Cheng Y. METTL3 promotes the proliferation and invasion of esophageal cancer cells partly through AKT signaling pathway. Pathol Res Pract 2020; 216: 153087.
[39] Han J, Wang JZ, Yang X, Yu H, Zhou R, Lu HC, Yuan WB, Lu JC, Zhou ZJ, Lu Q, Wei JF and Yang H. METTL3 promote tumor proliferation of bladder cancer by accelerating pri-miR221/222 maturation in m6A-dependent manner. Mol Cancer 2019; 18: 110.
[40] Horiuchi K, Kawamura T, Iwanari H, Ohashi R, Naito M, Kodama T and Hamakubo T. Identification of Wilms' tumor 1-associating protein complex and its role in alternative splicing and the cell cycle. J Biol Chem 2013; 288: 33292-33302.
[41] Batista PJ, Molinie B, Wang J, Qu K, Zhang J, Li L, Bouley DM, Lujan E, Haddad B, Daneshvar K, Carter AC, Flynn RA, Zhou C, Lim KS, Dedon P, Wernig M, Mullen AC, Xing Y, Giallourakis CC and Chang HY. m(6)A RNA modification controls cell fate transition in mammalian embryonic stem cells. Cell Stem Cell 2014; 15: 707-719.
[42] Luo H, Liu W, Zhang Y, Yang Y, Jiang X, Wu S and Shao L. METTL3-mediated m(6)A modification regulates cell cycle progression of dental pulp stem cells. Stem Cell Res Ther 2021; 12: 159.
[43] Petrachkova T, Wortinger LA, Bard AJ, Singh J, Warga RM and Kane DA. Lack of cyclin B1 in zebrafish causes lengthening of G2 and M phases. Dev Biol 2019; 451: 167-179.
[44] Bartel F, Taubert H and Harris LC. Alternative and aberrant splicing of MDM2 mRNA in human cancer. Cancer Cell 2002; 2: 9-15.
[45] Xiao W, Adhikari S, Dahal U, Chen YS, Hao YJ, Sun BF, Sun HY, Li A, Ping XL, Lai WY, Wang X, Ma HL, Huang CM, Yang Y, Huang N, Jiang GB, Wang HL, Zhou Q, Wang XJ, Zhao YL and Yang YG. Nuclear m(6)A reader YTHDC1 regulates mRNA splicing. Mol Cell 2016; 61: 507-519.
[46] Kasowitz SD, Ma J, Anderson SJ, Leu NA, Xu Y, Gregory BD, Schultz RM and Wang PJ. Nuclear m6A reader YTHDC1 regulates alternative polyadenylation and splicing during mouse oocyte development. PLoS Genet 2018; 14: e1007412.
[47] Patton JG, Porro EB, Galceran J, Tempst P and Nadal-Ginard B. Cloning and characterization of PSF, a novel pre-mRNA splicing factor. Genes Dev 1993; 7: 393-406.
[48] Marko M, Leichter M, Patrinou-Georgoula M and Guialis A. hnRNP M interacts with PSF and p54(nrb) and co-localizes within defined nuclear structures. Exp Cell Res 2010; 316: 390-400.
[49] Kim KK, Kim YC, Adelstein RS and Kawamoto S. Fox-3 and PSF interact to activate neural cell-specific alternative splicing. Nucleic Acids Res 2011; 39: 3064-3078.
[50] Melton AA, Jackson J, Wang J and Lynch KW. Combinatorial control of signal-induced exon repression by hnRNP L and PSF. Mol Cell Biol 2007; 27: 6972-6984.
[51] Song H, Wang Y, Wang R, Zhang X, Liu Y, Jia G and Chen PR. SFPQ is an FTO-binding protein that facilitates the demethylation substrate preference. Cell Chem Biol 2020; 27: 283-291, e6.
[52] Yue Y, Liu J, Cui X, Cao J, Luo G, Zhang Z, Cheng T, Gao M, Shu X, Ma H, Wang F, Wang X, Shen B, Wang Y, Feng X, He C and Liu J. VIRMA mediates preferential m(6)A mRNA methylation in 3'UTR and near stop codon and associates with alternative polyadenylation. Cell Discov 2018; 4: 10.
[53] Elcheva IA, Wood T, Chiarolanzio K, Chim B, Wong M, Singh V, Gowda CP, Lu Q, Hafner M, Dovat S, Liu Z, Muljo SA and Spiegelman VS. RNA-binding protein IGF2BP1 maintains leukemia stem cell properties by regulating HOXB4, MYB, and ALDH1A1. Leukemia 2020; 34: 1354-1363.